JACS
JOURNAL OF THE AMERICAN CHEMICAL SOCIETY
Article
pubs.acs.org/JACS

Structural Stability, Acidity, and Halide Selectivity of the Fluoride Riboswitch Recognition Site

Mohit Chawla,[†] Raffaele Credendino,[†] Albert Poater,[†,‡] Romina Oliva,[§] and Luigi Cavallo*[,†]

[†]KAUST Catalysis Research Center, Physical Sciences and Engineering Division, King Abdullah University of Science and Technology, Thuwal 23955-6900, Kingdom of Saudi Arabia

[‡]Institut de Química Computacional i Catàlisi and Departament de Química, Universitat de Girona, 17004 Girona, Spain

[§]Department of Sciences and Technologies, University "Parthenope" of Naples, Centro Direzionale Isola C4 80143, Naples, Italy

Supporting Information

ABSTRACT: Using static and dynamics DFT methods we show that the Mg^{2+}/F^{-}/phosphate/water cluster at the center of the fluoride riboswitch is stable by its own and, once assembled, does not rely on any additional factor from the overall RNA fold. Further, we predict that the pK_a of the water molecule bridging two Mg cations is around 8.4. We also demonstrate that the halide selectivity of the fluoride riboswitch is determined by the stronger Mg−F bond, which is capable of keeping together the cluster. Replacing F^{-} with Cl^{-} results in a cluster that is unstable under dynamic conditions. Similar conclusions on the structure and energetics of the cluster in the binding pocket of fluoride-inhibited pyrophosphatase suggest that the peculiarity of fluoride is in its ability to establish much stronger metal-halide bonds.

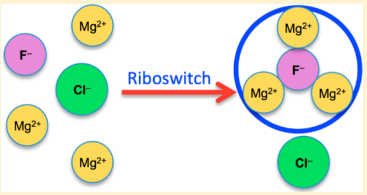

INTRODUCTION

Effective molecular recognition is prodromic for specificity and, in turn, functionality. This concept applies to practically all fields of science, from selectivity in catalysis, to sensoring in nanotechnology, to life processes. In this respect, the regulation of gene expression controlled by riboswitches is among the most recent novelties in the field. Riboswitches are short mRNA segments in the 5′-untranslated region, deputed to control gene expression by their expression platform, in response to the selective binding of a metabolite to their aptamer region; see Scheme 1.[1]

Scheme 1. (a) Inhibition or (b) Activation of Gene Expression Mediated by Metabolite Binding to Riboswitches

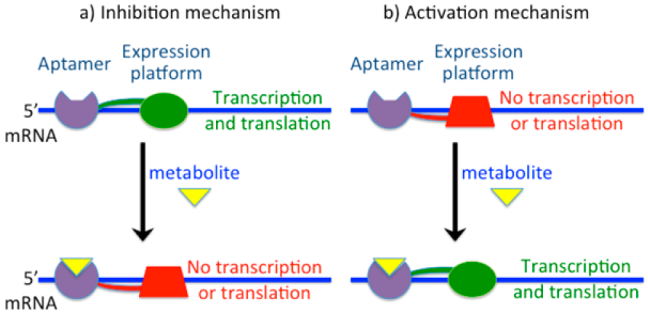

Currently, over 20 classes of riboswitches have been validated, targeting purines and analogues,[2−7] amino acids,[8−10] more complex metabolites,[11−17] or even simple Mg^{2+} cations.[18] Barring few exceptions,[19] metabolites recognized by the aptamer domain of riboswitch molecules are either neutral or positively charged, thus not preventing or even favoring the interaction of the metabolite with the negatively charged RNA backbone. Remarkably, a simple negatively charged fluoride anion has been recently added to the list of ligands targeted by riboswitches.[20]

Fluoride sensing riboswitches, characterized by a *crcB* structural motif and common to bacterial and archaeal species, have been shown to regulate the expression of genes that encode fluoride exporters.[21] Beside their capability to target the small fluoride anion with good efficiency, they remarkably reject other small anions, including chloride. A crystallographic structure has been recently solved for the fluoride-bound form of riboswitch from *Thermotoga petrophila*, whose affinity for fluoride (K_d of 135 ± 9 μM under 5 mM Mg^{2+}) and halide selectivity (no chloride binding observed in the presence of KCl) has been experimentally proved (PDB ID: 4ENC).[22] This structure evidenced that, in the middle of a pseudoknot scaffold, the fluoride is the central unit keeping together a small cluster of three Mg^{2+} cations, see Figure 1, whose coordination sphere is completed by oxygen atoms of five inwardly pointing backbone phosphate groups (some of them bridging two Mg^{2+} ions) from two distinct segments of the riboswitch sequence, and by water molecules, one of them bridging two of the Mg^{2+} ions.

The high fluoride selectivity and the structure of the recognition site in the fluoride riboswitch raises a series of questions. Among them are the following: (i) Is the small Mg^{2+}/F^{-}/phosphate/water cluster at the center of the riboswitch a stable entity on its own? (ii) Considering that water molecules bridging metal cations are known to be quite acidic,[23−28] what is the acidity of the water molecule bridging

Received: October 14, 2014
Published: December 8, 2014

DOI: 10.1021/ja510549b
J. Am. Chem. Soc. 2015, 137, 299−306

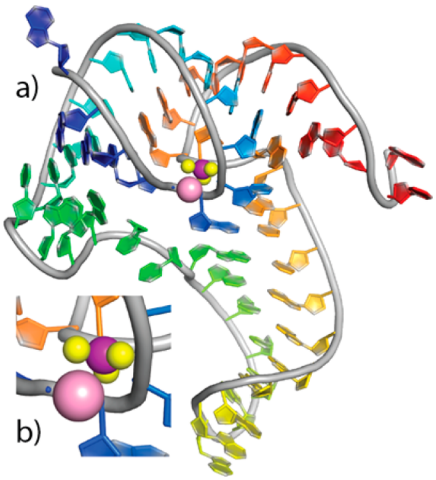

Figure 1. Schematic representation of the fluoride riboswitch in a rainbow spectrum, from 5′ end (blue) to 3′ end (red). Yellow and purple spheres, Mg^{2+} and F^- ions of the central cluster. Pink sphere, the K^+ ion.

two Mg^{2+} cations in the F-cluster at the center of the fluoride riboswitch? (iii) What is the origin of the halide selectivity? In this paper, we provide a clear answer to the above three fundamental questions, based on static and dynamic density functional theory (DFT) calculations. On the basis of analogous theoretical methods, we investigated the interaction of nucleic acid bases with metals[29] and we could recently decompose the binding of the preQ1 metabolite by the *Lactobacillus rhamnosus* class II preQ1 riboswitch.[30]

COMPUTATIONAL METHODS

Static Calculations. All the static DFT calculations (simply referred as DFT in the following) were performed with the Gaussian09 package.[31] The B3LYP functional,[32] with the addition of the D3 empirical dispersion term proposed by Grimme,[33] was used for all the calculations. The electronic configuration of the systems was described with the triple-ζ TZVP basis set.[34] Solvent effects, water, were included with the continuum solvation model CPCM.[35] Two different protocols were followed in the geometry optimizations. The first corresponding to standard gas-phase optimization, the second corresponding to in solvent optimizations, with water modeled with the CPCM model. The reported in solvent free energies were built through single point energy calculations on the B3LYP/TZVP optimized geometries using the M06 functional[36] and the triple-ζ TZVP basis function on all the atoms and the more extended def2-TZVPD basis set,[37] which include diffuse functions for oxygen, nitrogen and halides.

Dynamics Calculations. All the molecular dynamics DFT calculations (referred are DFT-MD in the following) were performed using the Born–Oppenheimer scheme as implemented in the CP2K Quickstep code.[38] The electronic structure calculations were carried out using the Perdew–Burke–Ernzerhof exchange and correlation functional,[39] with the addition of the D3 empirical dispersion term.[33] The CP2K program employs a mixed basis set approach with Gaussian-type orbitals (GTO) and plane waves (PWs).[38] GTO functions are used to expand the molecular orbitals and the charge density in real space, whereas PWs are used for the representation of the charge density in reciprocal space. An energy cutoff of 300 Ry is used for the plane-waves basis set. The GTH-DZVP double-ζ basis set with a polarization function, in conjunction with the Goedecker–Teter–Hutter pseudopotentials,[40] was used for all the atoms.

To start the DFT-MD simulations, the Gaussian09 optimized clusters were soaked in 267 water molecules in a cubic box of 20 $Å^3$. Water molecules clashing with the cluster atoms were removed. The systems were first equilibrated at 300 K for 1 ps in the NVT ensemble, by fixing the heavy atoms of the cluster, followed by another 1 ps equilibration by relaxing also the position of the heavy atoms of the cluster. A production run was then carried out for 10 ps in the NVT ensemble. The equations of motion were integrated using a time step of 0.5 fs. Temperature was controlled using a canonical-sampling-through-velocity-rescaling thermostat.[41] Movies of the dynamics are reported as Web-Enhanced Supporting Information. For the sake of clarity, solvent water molecules were removed when preparing the movies.

RESULTS AND DISCUSSION

DFT Modeling of the F-Riboswitch. To address the structural stability of the Mg^{2+}/F^-/phosphate/water cluster at the center of the fluoride riboswitch, we performed a series of geometry optimizations, both in the gas-phase and in water, modeled with a continuum solvation model, of different clusters of increasing size, from 87 atoms in the smallest model **1**, to 141 atoms in the largest model **13**. As in the crystallographic structure a water molecule is H-bonded to the Mg-bridging water, we considered different models in presence (entries **5**–**8** in Table 1, labeled as W models) or in the absence (entries **1**–**4** in Table 1) of this additional water molecule. Further, considering that in the crystallographic structure a K^+ ion from the K-acetate buffer is placed 4 Å away of the fluoride,[22] we increased the systems to include this K^+ ion and the phosphate group bound to it (entries **9**–**12** in Table 1, labeled as WK models). Finally, the largest system we considered includes the riboses connecting the phosphates coordinated to the Mg atoms (entry **13** in Table 1, labeled as WKS model). To mimic the constraint of the crystallographic

Table 1. Description of the Mg^{2+}/F^-/Phosphate/Water Cluster Models and Mean Unsigned Deviation, MUD in Å, of the Optimized Model from the X-ray Distances of Figure 1

	size[a]	CR[b]	solv[c]	MUD_a[d]	MUD_F[e]	MUD_O[e]	F_{out}[f]
1	–	Rlx	gas	0.49	0.18	2.00	0.21
2	–	Frz	gas	0.28	0.19	0.35	0.03
3	–	Rlx	water	0.24	0.19	0.20	0.04
4	–	Frz	water	0.25	0.21	0.21	0.01
5	W	Rlx	gas	0.18	0.16	0.12	0.04
6	W	Frz	gas	0.21	0.17	0.17	0.04
7	W	Rlx	water	0.22	0.18	0.15	0.04
8	W	Frz	water	0.23	0.20	0.15	0.01
9	WK	Rlx	gas	0.20	0.18	0.12	0.03
10	WK	Frz	gas	0.23	0.20	0.16	0.02
11	WK	Rlx	water	0.23	0.20	0.16	0.05
12	WK	Frz	water	0.22	0.20	0.12	0.01
13	WKS	Rlx	water	0.20	0.18	0.10	0.08

[a]Indicates if the crystallographic water molecule H-bonded to the Mg-bridging water is included in the model (W), if the K^+ ion is also included (WK), and if the riboses connecting the phosphates are also included (WKS). [b]Indicates if the position of the C3′ and C5′ atoms of the ribose was relaxed or frozen in the geometry optimization. [c]Indicates if solvent effects were included in the geometry optimization. [d]MUD_a is the mean unsigned deviation of the Mg–F, Mg–O (bridging water) and Mg–Mg distances from the crystallographic values. [e]MUD_F and MUD_O is the mean unsigned deviation of the Mg–F and Mg–O (bridging water) distances from the crystallographic values. [f]F_{out} is the deviation of the displacement of the F atom out of the plane of the three Mg atoms, from the crystallographic value.

DOI: 10.1021/ja510549b
J. Am. Chem. Soc. 2015, 137, 299–306

structure, in some of the models (labeled as "Frz" in Table 1) the ribose C3′ and C5′ atoms were frozen. In all cases the models were truncated to have an overall neutral charge. The mean unsigned deviation (MUD) of key interatomic distances and of the displacement of the F atom out of the plane of the three Mg atoms (F_{out}) in the optimized models, from the X-ray values, are reported in Table 1.

The main conclusions deriving from these calculations can be summarized as follows: (i) Geometry optimization in the gas-phase of the simple Mg^{2+}/F^{-}/phosphate/water cluster, in the absence of the water H-bonded to the Mg-bridging water, models **1**−**2** in Table 1, results in a clear deformation of the cluster, with the Mg-bridging water basically unable to keep together the two Mg cations effectively, as indicated by the rather large MUD_O. Inclusion of the solvent with the continuum solvation model CPCM, models **3**−**4** in Table 1, results in a stable cluster, with an overall MUD_a of 0.24−0.25 Å. (ii) Addition to the model of the crystallographic water molecule H-bonded to the Mg-bridging water results in overall stable clusters, with MUD_a in the 0.18−0.23 Å range, models **5**−**8** in Table 1. (iii) Enlarging the model to include the K^+ cation together with the bound phosphate, models **8**−**12** in Table 1, does not improves significantly the agreement with the X-ray structure. This indicates a minor impact of K^+ in determining the cluster structure, consistently with the experimental evidence that the K^+ ion does not interact with the fluoride.[22] (iv) Inclusion of the riboses connecting the phosphates bound to the Mg atoms has again minimal structural impact on the optimized geometry, model **13** in Table 1.

Figure 2 shows the optimized structure of models **7**, **11** and **13**, superimposed to the X-ray structure, highlighting the good overlap between the completely DFT optimized models and the crystallographic structure, independent of the model size.

Quantitatively, increasing the size of the model results in a slightly better agreement with the experimental structure, RMSD on the heavy atoms of 0.58, 0.68, and 0.44 Å for models **7**, **11** and **13**, respectively. The somewhat higher RMSD of model **11** is due to a movement of the dangling phosphate bound to the K^+ ion. Removing it from the fitting the RMSD of model **11** is 0.57 Å, similar to that of model **7**. This displacement of the dangling phosphate in model **11** is recovered when the riboses connecting the phosphates are included, as in model **13**. As for the average displacement of the C3′ and C5′ atoms in the optimized structures from the crystallographic structure, it amounts to 0.73 ± 0.56 Å, in model **7**, and it is reduced to only 0.38 ± 0.32 in model **13**. As for the displacement of the F atom out of the plane of the three Mg atoms, all models excellently reproduce the experimental value of 0.31 Å in the native crystallographic structure 4ENC (deviations clearly lower than 0.1 Å), with the exception of the wrong model **1**. Finally, in both models **11** and **13** the K^+ ion is pushed roughly 1 Å away from the mean coordination plane of the fluoride. Overall, the above analysis indicates that even the simpler model **7**, without the K^+ atom and the riboses connecting the phosphates, is substantially able to replicate the crystallographic structure to a very good extent, with deviations from the experimental structure comparable to those of the more extended models **11** and **13**.

However, during the gas phase DFT optimization of model **5**, we observed the transfer of one proton from the Mg-bridging water molecule to the H-bonded water, see Figure S1, and the best agreement with the crystallographic structure, with a

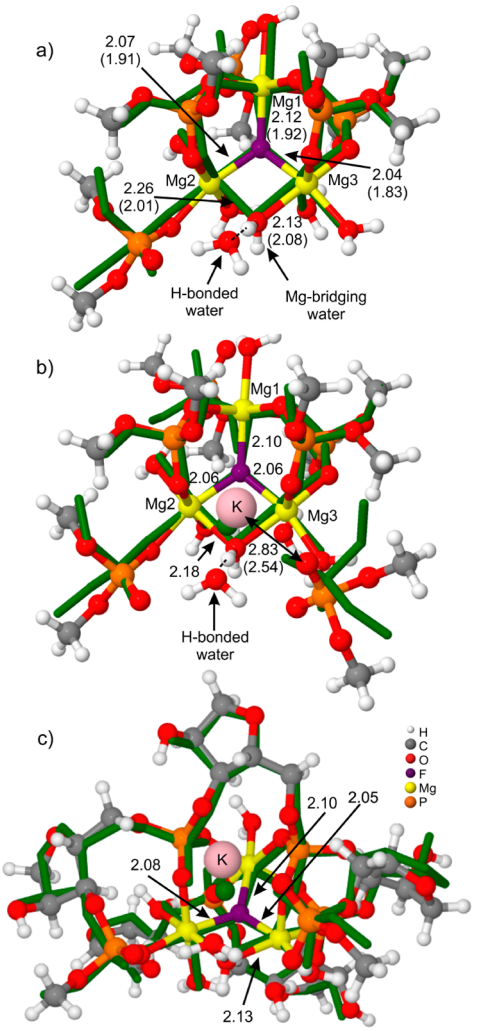

Figure 2. Superimposition of the optimized structure of models **7**, **11** and **13** of Table 1, stick and ball, with the crystallographic structure of the Mg^{2+}/F^{-}/phosphate/water cluster in 4ENC, green wireframe. Selected DFT and X-ray distances in Å, X-ray values in round parentheses.

MUD_a of 0.18 Å. Intrigued by this finding, and having in mind that a water molecule coordinated to two metal ions can be quite acidic,[23−28] we decided to optimize the geometry of models **1**−**13**, this time with a hydroxyl group bridging the Mg cations. In this case, the overall model is negatively charged. Deviation from the experimental structure is reported in Table 2.

The first result is that with a bridging hydroxide all the DFT optimization protocols resulted in a stable cluster. While it is not surprising that a hydroxyl group is able to keep together the cluster, the overall agreement with the crystallographic structure, with a MUD_a 0.17−0.20 Å, is comparable to that calculated in the presence of a Mg-bridging water molecule, with a MUD_a 0.18−0.23 Å.

As for a comparison between the different models, inclusion of K^+, models **9**−**12**, as well as of the riboses connecting the phosphates, model **13**, does not impact significantly the structure, as already found for the models with a Mg-bridging water molecule, compare entries **5**−**13** in Tables 1 and 2. Further, also in the presence of a Mg-bridging hydroxyl group, the displacement of the fluoride from the Mg atoms plane

DOI: 10.1021/ja510549b
J. Am. Chem. Soc. 2015, 137, 299−306

Table 2. Description of the Mg^{2+}/F^{-}/Phosphate/Hydroxide Cluster Models and Mean Unsigned Deviation, MUD in Å, of the Optimized Model from the X-ray Distances of Figure 1

	size[a]	CR[b]	solv[c]	MUD_a[d]	MUD_F[e]	MUD_O[e]	F_{out}[f]
1	–	Rlx	gas	0.18	0.18	0.08	0.01
2	–	Frz	gas	0.17	0.17	0.10	0.08
3	–	Rlx	water	0.18	0.18	0.06	0.05
4	–	Frz	water	0.19	0.19	0.08	0.03
5	W	Rlx	gas	0.18	0.18	0.11	0.01
6	W	Frz	gas	0.18	0.18	0.07	0.04
7	W	Rlx	water	0.18	0.18	0.05	0.03
8	W	Frz	water	0.18	0.19	0.06	0.02
9	WK	Rlx	gas	0.19	0.18	0.07	0.03
10	WK	Frz	gas	0.19	0.19	0.07	0.02
11	WK	Rlx	water	0.19	0.19	0.06	0.02
12	WK	Frz	water	0.20	0.21	0.07	0.02
13	WKS	Rlx	water	0.19	0.19	0.07	0.06

[a]Indicates if the crystallographic water molecule H-bonded to the Mg-bridging hydroxide is included in the model (W), if the K^+ ion is also included (WK), and if the riboses connecting the phosphates are also included (WKS). [b]Indicates if the position of the C3′ and C5′ atoms of the ribose was relaxed or frozen in the geometry optimization. [c]Indicates if solvent effects were included in the geometry optimization. [d]MUD_a is the mean unsigned deviation of the Mg−F, Mg−O (bridging hydroxide) and Mg−Mg distances from the crystallographic values. [e]MUD_F and MUD_O is the mean unsigned deviation of the Mg−F and Mg−O (bridging hydroxide) distances from the crystallographic values. [f]F_{out} is the deviation of the displacement of the F atom out of the plane of the three Mg atoms, from the crystallographic value.

reproduces excellently the experimental value. Overall, these results indicate that the crystallographic structure is also perfectly consistent with a Mg-bridging hydroxide.

DFT-MD Simulations of the F-Riboswitch. To test the cluster stability under dynamic conditions, we collected 10 ps long DFT-MD simulations, both considering water and hydroxide as Mg-bridging ligand, model 7 in Tables 1 and 2, as well as considering the analogous models in the presence of K^+, model **11** in Tables 1 and 2. In this case, the dangling phosphate bound to the K^+ was removed from the model. In all cases the cluster was soaked in a simulation box with about 250 water molecules, see the Computational Methods. Focusing on the cluster with a Mg-bridging water, the overall structure remains stable along the whole simulation, with the two Mg-water distances on the average 2.27 ± 0.13 Å, see Figure 3a. Similar small fluctuations were observed for the Mg−F distances, see again Figure 3a, with an average value of 2.14 ± 0.12 Å, and for the displacement of the fluoride out of the Mg atoms plane, 0.28 ± 0.09 Å. Inclusion of the K^+ cation has minimal impact on the dynamic behavior of the system, with average values for the Mg-water and Mg−F distances of 2.22 ± 0.10 and 2.12 ± 0.11 Å. The only anomaly in the dynamics is the isolated peak in the Mg2−F distance around 4 ps, see Figure 3b, while the Mg−O distances remains clearly stable along the whole trajectory, see again Figure 3b. To check if this peak is indicative of dynamic instability, we elongated the MD trajectories both in the absence as well as in the presence of the K^+ cation up to 20 ps, see Figure S2, but no other sign of instability was observed. This indicates that the simple Mg^{2+}/F^{-}/phosphate/water cluster is a remarkably stable structure on its own that, once achieved, does not need higher-order

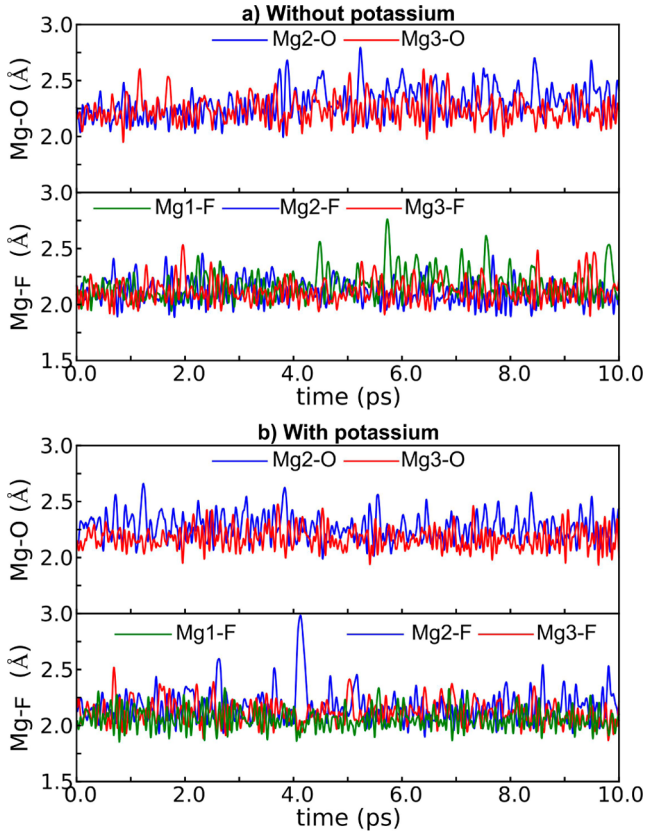

Figure 3. Time evolution of the Mg−O and Mg−F distances during the DFT-MD simulation of the Mg^{2+}/F^{-}/phosphate/water cluster (a), and of the same distances during the DFT-MD simulation of the same cluster in the presence of a K^+ ion (b).

stabilizing effects, like the whole RNA backbone structure, to be held in place. The corresponding plots for the cluster bearing a hydroxide Mg-bridging group, with average values for the Mg−OH and Mg−F distances of 2.06 ± 0.08 and 2.11 ± 0.10 Å in the absence of the K^+ ion, and 2.02 ± 0.07 and 2.10 ± 0.10 Å in the presence of the K^+ ion, show similar stability, and thus we do not discuss them in details, see Figure S3 for a plot.

DFT Prediction of the Acidity of the F-Riboswitch. At this point, we investigated the potential acidity of the Mg-bridging water molecule, as indicated in eq 1.

$$[\text{F-cluster}(H_2O)] + H_2O \rightarrow [\text{F-cluster}(OH)]^- + H_3O^+ \quad (1)$$

Since the absolute prediction of the pK_a of an aquaion by DFT is prone to several sources of error,[42] we calibrated a protocol by fitting the DFT calculated pK_a of a series of mono aquaions with charge +1 to +3 to the experimental pK_a. The developed protocol was validated in the prediction of the pK_a of a water molecule in a dinuclear Ni-complex, used as model of the dinuclear Ni-cluster in urease,[43] see the Supporting Information for details. According to these calculations, the predicted pK_a of the riboswitch, estimated as the average of the predicted pK_a in selected models, see Table 3, is 8.4, which is clearly lower than 11.4, the experimental pK_a of $[Mg(H_2O)_6]^{2+}$.[44] While it would be purely speculative to imagine any functional role for this quite acidic Mg-bridging water, we remark that at the physiologic pH = 7, a pK_a of 8.4 corresponds to having a sizable fraction of the riboswitch with a Mg-bridging hydroxyl group.

DOI: 10.1021/ja510549b
J. Am. Chem. Soc. 2015, 137, 299−306

Table 3. Predicted pKa of Selected Models of the Central Cluster of the F-Riboswitch, Together with the Average Value

model	7	8	11	12	13	avg
pK_a	8.6	8.6	9.1	7.4	8.1	8.4

DFT and DFT-MD Simulation of the Cl-Riboswitch. Finally, we focused on the halide selectivity of the riboswitch, by investigating Cl^- binding. Optimization of the Mg^{2+}/Cl^-/phosphate/water cluster (with a computational protocol corresponding to models **7**, **11** and **13** of Tables 1 and 2) results in a fairly stable structure with no evident deformation of the system, see Figure S4. The Mg-bridging water is firmly held in place even in the cluster corresponding to the small model **7**, MUD_O 0.20 Å (versus 0.16 Å in the F-cluster, entry 7 Table 1), while the MUD_{Cl} of 0.68 Å reflects the longer Mg−Cl versus Mg−F bonds, on the average 2.56 versus 2.07 Å, respectively. Similar stability is found for the Mg-bridging hydroxide clusters, see again the Supporting Information. This may suggest that the riboswitch could be able to fold and coordinate the Cl^- ion. To test the cluster under dynamic conditions, also in this case we performed DFT-MD simulations of the clusters corresponding to models **7** and **11**. Analysis of the Mg−Cl and Mg-bridging water distances in the absence of the K^+ ion indicates a clear instability of the Mg^{2+}/Cl^-/phosphate/water cluster under dynamic conditions, see Figure 4a. Indeed, after 1 ps of rather stable behavior, severe fluctuations occurs in both the Mg3−O and Mg1−Cl bonds, with the Mg1 atom almost flying away from the cluster, see the snapshot in Figure 5, other two snapshots are reported in Figure S5.

Inclusion of K^+ in the dynamics results in a more stable behavior of the cluster. Nevertheless, large fluctuations of the Mg3-water (around 2.2 and 5.5 ps) and Mg3−Cl (around 5 and beyond 6 ps) distances, see Figure 4b, together with an average value of the Mg-water distances of 2.39 ± 0.22 Å, as compared to the value of 2.22 ± 0.10 Å in the corresponding dynamics of the F-cluster, can still be taken as clear signals of some structural instability of the Cl-water cluster also in the presence of the K^+ ion.

The DFT-MD simulation of the Cl-clusters presenting a Mg-bridging hydroxide group results in quite stable Mg−OH distance, with an average value of 2.04 ± 0.07 in the absence of K^+, and of 2.05 ± 0.07 Å in the presence of K^+, see Figure S6. Differently, the Mg−Cl distances show large fluctuations, particularly in the absence of K^+, with average values of 2.81 ± 0.26 and 2.71 ± 0.16 Å, see again Figure S6. The higher stability of the cluster in the presence of a Mg-bridging hydroxide is not surprising, due to the clearly stronger Mg−OH bond compared to the Mg-water bond. Indeed, the dynamic simulation of the Mg-bridging water Cl-clusters highlighted the longer Mg−O distances as points of weakness. Although a limited number of short simulations does not allow for definitive conclusions, the larger fluctuations or even the disruption of the Cl-cluster in some of the simulations contrasts with the clear stability of the F-cluster up to 20 ps. This illuminates that the selectivity of the riboswitch in favor of F^- (or better the inability of the riboswitch to bind halides other than F^-) is related to the structural instability of the core Mg^{2+}/heavier halide/phosphate/water cluster.

DFT Estimation of the F−Mg and Cl−Mg Bond Energy. To quantify the difference of F^- versus Cl^- binding,

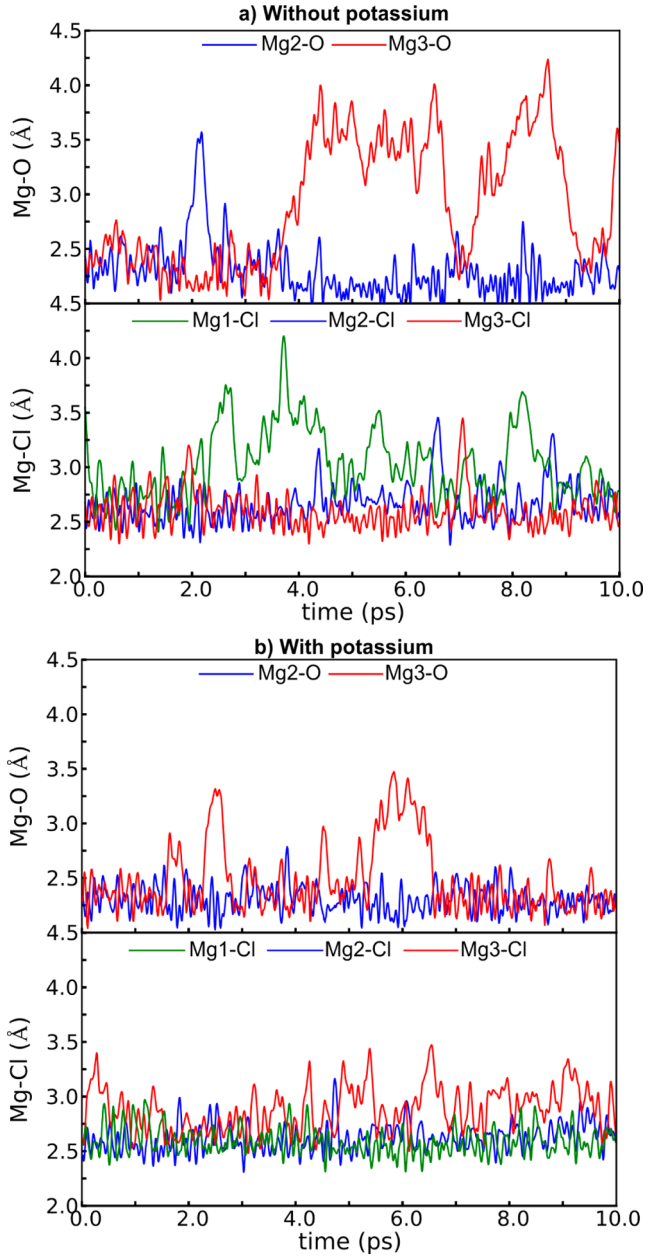

Figure 4. Time evolution of the Mg−O and Mg−Cl distances during the DFT-MD simulation of the Mg^{2+}/Cl^-/phosphate/water cluster (a), and of the same distances during the DFT-MD simulation of the same cluster in the presence of a K^+ ion (b).

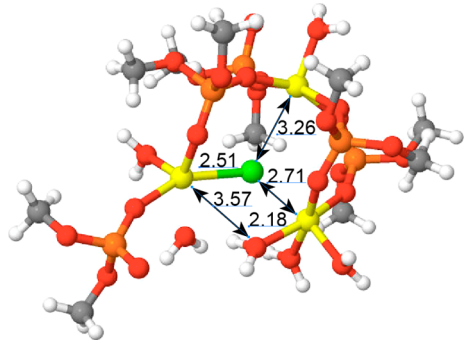

Figure 5. Selected frame from the DFT-MD simulation of the Cl-cluster at 2.18 ps. Key distances in Å.

DOI: 10.1021/ja510549b
J. Am. Chem. Soc. 2015, 137, 299−306

we evaluated the halide substitution energy in water, using the largest considered model **13**, as indicated in eq 2.

$$\text{Ribosw-F} + \text{Cl}^- \rightarrow \text{Ribosw-Cl} + \text{F}^- + \Delta G_{sub} \quad (2)$$

where Ribosw-F and Ribosw-Cl are the Mg^{2+}/X^-/phosphate/water clusters (X = F, Cl). According to the DFT protocol adopted in this work, the left side of eq 2 is favored by 47.1 kcal/mol, indicating that the fluoride bound cluster is clearly more stable, despite the remarkably stronger solvation of the free F^- would favor its substitution by Cl^-.[45] To unravel if the instability of the Cl-cluster is due to internal strain, consequence of the longer Mg−Cl bonds that stress the phosphate and water bridges connecting the Mg atoms, or it is consequence of the intrinsic weakness of the Mg−Cl bond compared to the Mg−F bond, we decomposed ΔG_{Sub} according to the hypothetical thermodynamic cycle of Figure 6.

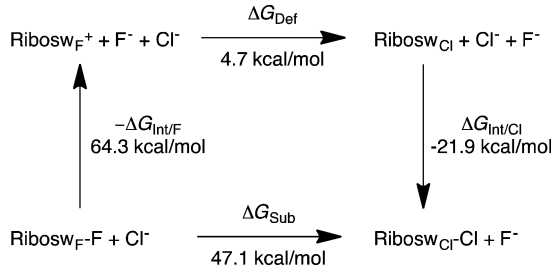

Figure 6. Thermodynamic cycle used to decompose the different stability of the F- and Cl-clusters.

The first vertical step of the cycle of Figure 6 corresponds to rigidly fragmenting the optimized F-cluster into the Ribosw$_F^+$ fragment and the F^- ion, where Ribosw$_F^+$ indicates the cluster (without the F^- ion) in the exact geometry it has in the optimized F-cluster, while the second vertical step of the cycle corresponds to rigidly combining the optimized Cl-cluster from the Ribosw$_{Cl}^+$ fragment and the Cl^- ion, where Ribosw$_{Cl}^+$ indicates the cluster (without the Cl^- ion) in the exact geometry it has in the optimized Cl-cluster. The top horizontal step of the cycle corresponds to deform the geometry of the fragment corresponding to the halide free cluster from the geometry it has in the F-cluster to the geometry it has in the Cl-cluster. The thermodynamic cycle of Figure 6 allows to decompose ΔG_{sub} as in eq 3.[46]

$$\Delta G_{Sub} = \Delta G_{Def} + \Delta G_{Int} = \Delta G_{Def} - \Delta G_{Int/F} + \Delta G_{Int/Cl} \quad (3)$$

where ΔG_{Def}, is the energy difference between the geometries of the Ribosw$_X^+$ fragment in the Ribosw-F and Ribosw-Cl clusters, while ΔG_{Int} is the difference in the interaction energy between the free halides and the Ribosw$_X^+$ fragments, $\Delta G_{Int/F}$ and $\Delta G_{Int/Cl}$. According to calculations, ΔG_{Def} amounts to only 4.7 kcal/mol, which indicates that strain in the phosphate and water bridges connecting the three Mg cations marginally destabilizes the Cl-cluster. On the other hand, the interaction energy between the Ribosw$^+$ and the X^- fragments amounts to 64.3 and 21.9 kcal/mol for F^- and Cl^-, for a ΔG_{Int} of 47.1 kcal/mol, indicating that the difference in stability between the F- and Cl-clusters can be almost totally ascribed to the different strength of the Mg−Cl and Mg−F bonds.

To have better insight into this difference, we calculated the Mg−X bond dissociation energy, BDE, in the $[Mg(H_2O)_5X]^+$ complexes (X = F, Cl), as indicated in eq 4.

$$[Mg(H_2O)_5X]^+ \rightarrow [Mg(H_2O)_5]^{2+} + X^- + \text{BDE} \quad (4)$$

According to calculations, the Mg−F bond, with a BDE of 37.3 kcal/mol, is 19.6 kcal/mol stronger than the Mg−Cl bond, with a BDE of 17.7 kcal/mol, despite solvation stabilizes more F^- than Cl^-,[45] further confirming that the instability of the Cl-cluster is dominated by the intrinsic weakness of the Mg−Cl bond.

DFT Modeling of the F-Inhibited Pyrophosphatase. Intrigued by these results, we decided to investigate the structure and the energetics of an analogous three metals cluster held together by a fluoride anion, as present in the crystallographic structure of fluoride-inhibited pyrophosphatase (PDB ID: 1E6A).[47] Similarly to the cluster at the center of the fluoride riboswitch, the binding pocket of the fluoride-inhibited pyrophosphatase system consists of the fluoride anion coordinated by three metal ions, specifically two Mn^{2+} and one Na^+ ion. The coordination sphere of the three metal ions is completed by the carboxylate side chain of four Asp residues and by five water molecules. In addition, the natural pyrophosphate (POP) substrate is bound to this binding pocket in the crystallographic structure. For these reasons, we decided to investigate structure and energetics of the F-centered cluster in this protein, using the same protocol used to investigate the cluster at the center of the fluoride riboswitch.

We cut two different models from the crystallographic structure. Besides the two Mn^{2+} (each considered in the hextet spin state), the Na^+ and the F^- ions, the first model includes the four metal bound Asp side chains (up to the Cβ), one POP ligand and the four water molecules completing the metals coordination sphere in the crystallographic structure. The position of the Cβ atom of the Asp side chains was frozen to mimic the experimental structure. Further, considering that three of the four Asp residues are close in sequence, amino acids 115, 117 and 120, the larger second model comprises the pyrophosphatase polypeptide backbone atoms from Asp115 to Asp120, including the Cβ atom of Asn116 and Ile119, and the full ring of Pro118. Considering the larger size of this model, and the presence of the whole Asp115 to Asp120 backbone, no atom position was constrained. Optimization was performed in water, modeled with the continuum solvation model CPCM.

Optimization of the first model results in fairly stable cluster with no evident deformation of the system, see Figure 7a, with a RMSD from the crystallographic structure of 0.85 Å. The fluoride ion is firmly held in place, with a MUD on the F-metal distances of 0.20 Å. Optimization of the larger model also results in a good agreement with the experimental structure, despite no constraint on the atoms position, with an overall RMSD of 0.63 Å on the heavy atoms, see Figure 7b. This suggests that the considered models are both able to capture the structure of the cluster. Replacing F^- with Cl^- has instead a strong impact on the cluster structure. Despite the constraint on the position of the Cβ atoms, optimization of the small model of the Cl-cluster results in clear deformation of the cluster, with the Cl^- ion losing its coordination from one of the Mn^{2+} ions and from the Na^+ ion, see Figure S7, and a RMSD of 1.17 Å from the crystallographic structure. Differently, optimization of the larger model results in an overall stable cluster, with a RMSD of 0.60 Å from the crystallographic structure, and with the M−Cl distances (M = Mn, Na) about 0.5 Å longer than the corresponding M−F optimized distance. This elongation of the M−X bond is similar to what we found in the case of the fluoride riboswitch.

DOI: 10.1021/ja510549b
J. Am. Chem. Soc. 2015, 137, 299−306

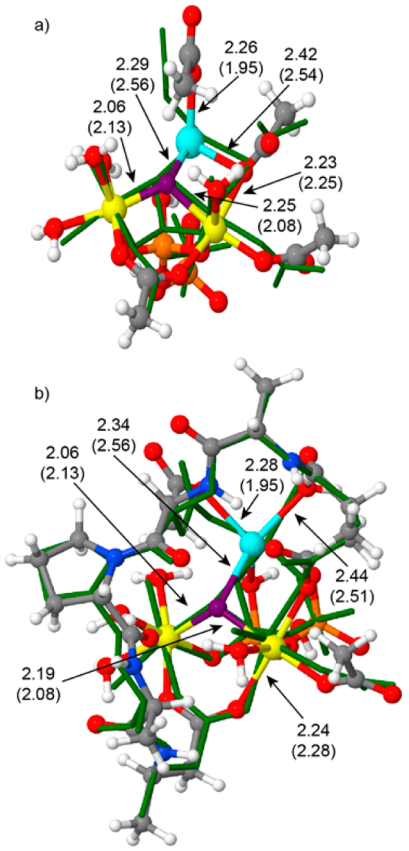

Figure 7. Superimposition of the DFT optimized structure of models of the F-cluster of pyrophosphatase, stick and ball, with the crystallographic structure of 1E6A, green wireframe. Selected DFT and X-ray distances in Å, X-ray values in round parentheses.

To shed light on the energetics connected to the binding of the halide at the center of the cluster, we calculated the halide substitution energy, according to eq 2, using the optimized geometry of the larger F- and Cl-clusters. According to the protocol we used, binding of F^- is favored by 25.9 kcal/mol, indicating that also in the case of the pyrophosphatase cluster, the binding of the fluoride is remarkably favored. To clarify the relative weight of the Mn−X versus the Na−X bond, we calculated the M−X bond dissociation energy in the $[Mn(H_2O)_5X]^+$ and $[Na(H_2O)_4X]$ complexes, as indicated in eq 4. According to these calculations, the Mn−F and Na−F bonds, with a BDE of 36.0 and 11.7 kcal/mol, are 12.5 and 7.1 kcal/mol stronger than the Mn−Cl and Na−Cl bond, with a BDE of 23.5 and 4.6 kcal/mol, respectively, indicating that the instability of the Cl-cluster is basically distributed on the Mn−Cl and Na−Cl bonds to almost a similar extent.

CONCLUSIONS

In conclusion, our analysis of the core Mg^{2+}/halide/phosphate/water cluster of the fluoride riboswitch from *T. petrophila* allowed to clearly explain the following: (i) The core cluster is a stable entity on its own, under both static and dynamic conditions. Once assembled, this structure does not need any additional stabilizing factor from the overall RNA molecule. (ii) Replacing the Mg-bridging water molecule with a hydroxyl group results in a structure perfectly consistent with the experimental data, although it should be considered that this requires having an overall negatively charged cluster, in the negatively charged environment provided by the RNA skeleton. (iii) The Mg-bridging water molecule is quite acidic, with a predicted pK_a around 8.4. (iv) Replacing the fluoride with a chloride in the DFT geometry optimization leads to minor structural changes, which indicates that binding of heavier halides could be structurally feasible. However, the DFT-MD simulations indicated that the Cl-cluster is unstable under dynamic conditions, with the substantial rupture of Mg−Cl and Mg-water bonds. (v) Binding of a fluoride in the core cluster of the riboswitch is clearly stronger than binding of a chloride, and this difference can be mainly ascribed to the difference in the Mg−F and Mg−Cl bonds strength. (vi) Calculations on the F-centered cluster of fluoride-inhibited pyrophosphatase show that also in this case fluoride has a much better ability than chloride to hold together the cluster, both from a structural and energetic point of view.

ASSOCIATED CONTENT

Supporting Information

Cartesian coordinates, details on the computational protocols, pK_a calculation, additional analysis, movies of the dynamic simulations. This material is available free of charge via the Internet at http://pubs.acs.org.

AUTHOR INFORMATION

Corresponding Author

luigi.cavallo@kaust.edu.sa

Notes

The authors declare no competing financial interest.

ACKNOWLEDGMENTS

We thank one of the reviewers for suggesting us to model the pyrophosphatase system. Research reported in this publication was supported by the King Abdullah University of Science and Technology. We thank the HPC team of Enea (www.enea.it) for generous access to the ENEA-GRID and the HPC facilities CRESCO (www.cresco.enea.it) in Portici, Italy. A.P. thanks the Spanish MINECO for a Ramón y Cajal contract (RYC-2009-05226) and European Commission for a Career Integration Grant (CIG09-GA-2011-293900).

REFERENCES

(1) Serganov, A.; Nudler, E. *Cell* **2013**, *152*, 17.
(2) Mandal, M.; Breaker, R. R. *Nat. Struct. Mol. Biol.* **2004**, *11*, 29.
(3) Sudarsan, N.; Lee, E. R.; Weinberg, Z.; Moy, R. H.; Kim, J. N.; Link, K. H.; Breaker, R. R. *Science* **2008**, *321*, 411.
(4) (a) Gilbert, S. D.; Mediatore, S. J.; Batey, R. T. *J. Am. Chem. Soc.* **2006**, *128*, 14214. (b) Gilbert, S. D.; Reyes, F. E.; Edwards, A. L.; Batey, R. T. *Structure* **2009**, *17*, 857.
(5) Smith, K. D.; Lipchock, S. V.; Ames, T. D.; Wang, J.; Breaker, R. R.; Strobel, S. A. *Nat. Struct. Mol. Biol.* **2009**, *16*, 1218.
(6) (a) Roth, A.; Winkler, W. C.; Requlski, E. E.; Lee, B. W.; Lim, J.; Jona, I.; Barrick, J. E.; Ritwik, A.; Kim, J. N.; Welz, R.; Iwata-Reuyl, D.; Breaker, R. R. *Nat. Struct. Mol. Biol.* **2007**, *14*, 308. (b) Liberman, J. A.; Salim, M.; Krucinska, J.; Wedekind, J. E. *Nat. Chem. Biol.* **2013**, *9*, 353.
(7) Batey, R. T.; Gilbert, S. D.; Montange, R. K. *Nature* **2004**, *18*, 411.
(8) Mandal, M.; Lee, M.; Barrick, J. E.; Weinberg, Z.; Emilsson, G. M.; Ruzzo, W. L.; Breaker, R. R. *Science* **2004**, *306*, 275.
(9) Serganov, A.; Huang, L.; Patel, D. J. *Nature* **2008**, *455*, 1263.
(10) Huang, L.; Serganov, A.; Patel, D. J. *Mol. Cell* **2010**, *40*, 774.
(11) Winkler, W. C.; Nahvi, A.; Sudarsan, N.; Barrick, J. E.; Breaker, R. R. *Nat. Struct. Mol. Biol.* **2003**, *10*, 701.
(12) Serganov, A.; Huang, L.; Patel, D. J. *Nature* **2009**, *458*, 233.

DOI: 10.1021/ja510549b
J. Am. Chem. Soc. 2015, 137, 299−306

(13) Gilbert, S. D.; Rambo, R. P.; Van Tyne, D.; Batey, R. T. *Nat. Struct. Mol. Biol.* **2008**, *15*, 177.
(14) Trausch, J. J.; Ceres, P.; Reyes, F. E.; Batey, R. T. *Structure* **2011**, *19*, 1413.
(15) Montange, R. K.; Batey, R. T. *Nature* **2006**, *441*, 1172.
(16) Roth, A.; Winkler, W. C.; Regulski, E. E.; Lee, B. W.; Lim, J.; Jona, I.; Barrick, J. E.; Ritwik, A.; Kim, J. N.; Welz, R.; Iwata-Reuyl, D.; Breaker, R. R. *Nat. Struct. Mol. Biol.* **2007**, *14*, 308.
(17) Liberman, J. A.; Salim, M.; Krucinska, J.; Wedekind, J. E. *Nat. Chem. Biol.* **2013**, *9*, 353.
(18) Wakeman, C. A.; Ramesh, A.; Winkler, W. C. *J. Mol. Biol.* **2009**, *392*, 723.
(19) (a) Winkler, W.; Nahvi, A.; Breaker, R. R. *Nature* **2002**, *419*, 952. (b) Barrick, J. E.; Corbino, K. A.; Winkler, W. C.; Nahvi, A.; Mandal, M.; Collins, J.; Lee, M.; Roth, A.; Sudarsan, N.; Jona, I.; Wickiser, J. K.; Breaker, R. R. *Proc. Natl. Acad. Sci. U. S. A.* **2004**, *101*, 6421. (c) Mironov, A. S.; Gusarov, I.; Rafikov, R.; Lopez, L. E.; Shatalin, K.; Kreneva, R. A.; Perumov, D. A.; Nudler, E. *Cell* **2002**, *111*, 747.
(20) Baker, J. L.; Sudarsan, N.; Weinberg, Z.; Roth, A.; Stockbridge, R. B.; Breaker, R. R. *Science* **2012**, *335*, 233.
(21) Li, S.; Smilth, K. D.; Davis, J. H.; Gordon, P. B.; Breaker, R. R.; Strobel, S. A. *Proc. Natl. Acad. Sci. U. S. A.* **2013**, *110*, 19018.
(22) Ren, A.; Rajashankar, K. R.; Patel, D. J. *Nature* **2012**, *486*, 85.
(23) Wilcox, D. E. *Chem. Rev.* **1996**, *96*, 2435.
(24) Samples, C. R.; Howard, T.; Raushel, F. M.; DeRose, V. J. *Biochemistry* **2005**, *44*, 11005.
(25) Park, J. M.; Boero, M. *J. Phys. Chem. B* **2010**, *114*, 11102.
(26) Hermann, T.; Auffinger, P.; Scott, W. G.; Westhof, E. *Nucleic Acids Res.* **1997**, *25*, 3421.
(27) Cama, E.; Pethe, S.; Boucher, J. L.; Han, S.; Emig, F. A.; Ash, D. E.; Viola, R. E.; Mansuy, D.; Christianson, D. W. *Biochemistry* **2004**, *43*, 8987.
(28) (a) Suarez, D.; Diaz, N.; Merz, K. M., Jr. *J. Am. Chem. Soc.* **2003**, *125*, 15324. (b) Salminen, T.; Kapyla, J.; Heikinheimo, P.; Kankare, J.; Goldman, A.; Heinonen, J.; Baykov, A. A.; Cooperman, B. S.; Lahti, R. *Biochemistry* **1995**, *34*, 782.
(29) (a) Oliva, R.; Cavallo, L. *J. Phys. Chem. B* **2009**, *113*, 15670−15678. (b) Oliva, R.; Tramontano, A.; Cavallo, L. *RNA* **2007**, *13*, 1427.
(30) Chawla, M.; Abdel-Azeim, S.; Oliva, R.; Cavallo, L. *Nucleic Acids Res.* **2014**, *42*, 714.
(31) *Gaussian*, Version 09.D1; Gaussian, Inc.: Wallingford, CT, 2009.
(32) (a) Becke, A. D. *J. Chem. Phys.* **1993**, *98*, 5648. (b) Becke, A. D. *J. Chem. Phys.* **1996**, *104*, 1040. (c) Lee, C.; Yang, W.; Parr, R. G. *Phys. Rev. B: Condens. Matter Mater. Phys.* **1988**, *37*, 785.
(33) Grimme, S.; Antony, J.; Ehrlich, S.; Krieg, H. *J. Chem. Phys.* **2010**, *132*, 154104.
(34) Godbout, N. D.; Salahub, R.; Andzelm, J.; Wimmer, E. *Can. J. Chem.* **1992**, *70*, 560.
(35) (a) Barone, V.; Cossi, M. *J. Phys. Chem. A* **1998**, *102*, 1995. (b) Cossi, M.; Rega, N.; Scalmani, G.; Barone, V. *J. Comput. Chem.* **2003**, *24*, 669.
(36) Zhao, Y.; Truhlar, D. G. *Theor. Chem. Acc.* **2008**, *120*, 215.
(37) Kaupp, M.; Schleyer, P. V.; Stoll, H.; Preuss, H. *J. Chem. Phys.* **1991**, *94*, 1360.
(38) VandeVondele, J. K. M.; Mohamed, F.; Parrinello, M.; Chassaing, T.; Hutter, J. *J. Comp. Phys. Comm.* **2005**, *167*, 103.
(39) Perdew, J. P.; Burke, K.; Ernzerhof, M. *Phys. Rev. Lett.* **1996**, *77*, 3865.
(40) Goedecker, S.; Teter, M.; Hutter, J. *Phys. Rev. B: Condens. Matter Mater. Phys.* **1996**, *54*, 1703.
(41) Bussi, G.; Donadio, D.; Parrinello, M. *J. Chem. Phys.* **2007**, *126*, 014101−1.
(42) (a) Gilson, R.; Durrant, M. C. *Dalton Trans.* **2009**, 10223. (b) Bryantsev, V. S.; Diallo, M. S.; Goddard, W. A., III *J. Phys. Chem. A* **2009**, *113*, 9559.
(43) Barrios, A. M.; Lippard, S. J. *J. Am. Chem. Soc.* **1999**, *121*, 11751.
(44) Richens, D. T. *The Chemistry of Aqua Ions*; John Wiley Ed.: New York, 1997.
(45) The default CPCM setup calculates the solvation energy of F^- and Cl^- to be −84.2 and −69.8 kcal/mol. Using the experimental values of −104.6 and −74.5 kcal/mol for F^- and Cl^-, the right side of eq 2 is favored by 30.8 kcal/mol.
(46) (a) Sponer, J.; Jurecka, P.; Hobza, P. *J. Am. Chem. Soc.* **2004**, *126*, 10142. (b) Oliva, R.; Cavallo, L.; Tramontano, A. *Nucleic Acids Res.* **2006**, *34*, 865.
(47) Heikinheimo, P.; Tuominen, V.; Ahonen, A. K.; Teplyakov, A.; Cooperman, B. S.; Baykov, A. A.; Lahti, R.; Goldman, A. *Proc. Natl. Acad. Sci. U. S. A.* **2001**, *98*, 3121.

DOI: 10.1021/ja510549b
J. Am. Chem. Soc. 2015, 137, 299−306